The Effects of Surfactants on the Motion and Transport Mechanisms of a Condensing Droplet in a High Reynolds Number Flow

The motion and transport mechanisms of a condensing droplet initially contaminated with insoluble monolayer surfactant material are examined through a theoretical approach. The surface tension gradient force induced by the surfactant and the shear stress from the relative motion between droplet and its ambient vapor are evaluated on the droplet surface as major forces affecting the internal motion of the droplet. The strength of the internal motion ranges from one order of magnitude smaller than the free stream velocity for slight surfactant contamination to almost a complete stop in motion for high surfactant concentration.

TAE-HO CHANG
and J. N. CHUNG

Department of Mechanical Engineering
Washington State University
Pullman, WA 99164-2920

SCOPE

It has been indicated by many review articles that only a small fraction of the published experimental results in the area of bubble and droplet transport phenomena agrees with the existing theory. Experimental liquids (especially water) are very easily contaminated with surface active materials (surfactants), which alter the surface tension and, therefore, a surface tension gradient along the interface develops. The internal motion of a bubble or droplet then is retarded and the convective heat and mass transfer rates are reduced.

Kintner (1963), Harper (1972), and Clift et al. (1978) have reviewed the literature on the effects of surfactants on the motion and transport mechanism of bubbles and droplets. They have found that almost all the research work has been done in the area of surfactant cap on a bubble in creeping flow conditions.

A comprehensive understanding of the role played by the monolayer surfactants on the fluid motion and the transport mechanisms of bubbles and droplets under phase change in high Reynolds number flows is of fundamental importance. For example, it will shed light on the following processes: the absorption of pollutant species by the condensing raindrops in the atmospheric science area, the effects of surfactants on the formation and motion of vapor bubbles in boiling heat transfer, two-phase flow, combustion of fuel droplets, spray drying, and direct contact heat and mass transfer. The nuclear industry also benefits from this study, as it will contribute to the design of the nuclear reactor containment spray system where surfactants are likely to be present.

In this study, the following effects have been examined specifically:

1. The effect of monolayer surfactant on the surface conditions, i.e., surface equilibrium conditions and surface tension distribution.
2. The effect of monolayer surfactant on the fluid motion inside the droplet.
3. The condition for the formation of surfactant cap from monolayer surfactant on the drop surface.

CONCLUSIONS AND SIGNIFICANCE

The effects of insoluble monolayer surfactants on the internal circulation of a condensing droplet in high Reynolds number flow have been investigated for droplet radii ranging from 100 to 1,000 μm. The surfactant surface diffusivity varies from 10^{-9} to 10^{-3} m^2/s.

It is found that surfactants with lower surface diffusion coefficients are more effective in weakening the strength of internal circulation. This may be explained by the convection-diffusion balanced transport mechanism on the surface. Droplets with more total amount of the same surfactant have slower internal motion because that much more surface area is under surfactant concentration gradients, which oppose the internal motion. The surfactant is found to be more effective on smaller droplets. It is shown that faster internal motion with larger surface diffusion coefficient will result in similar surfactant concentration distribution to that of slower internal motion with a smaller surface diffusion coefficient. Since the concentration distribution is governed by the surface Peclet number, $Pe_s = R \cdot AR^2/D_s$ (R is the droplet radius, AR^2 is the strength of internal motion, and D_s is the diffusion coefficient), for a given droplet size, the strength of internal circulation is balanced by the surface diffusion coefficient. In general, surfactant concentration rises sharply after the equator, and the strength of the internal motion ranges from one order of mag-

nitude smaller than the free stream velocity for slight surfactant contamination to almost a complete stop in motion for high surfactant contamination. The total drag coefficient decreases with increasing internal circulation.

The current study provides fundamental understanding of the effects of insoluble monolayer surfactant on the internal motion of condensing droplets that are seen in any important transport processes.

LITERATURE REVIEW

The motion of a fluid sphere in another immiscible fluid was first solved theoretically by Hadamard (1911) and Rybczynski (1911) for low Reynolds number flow where the inertia term was neglected. Also neglected in their analyses was the existence of surface active material. The continuity of shear stress and tangential velocity were the interfacial conditions. But their results were not confirmed by experiments (Harper, 1972). This led Boussinesq (1912) to hypothesize that a skin that inhibits the internal circulation can form around a moving droplet. He obtained an exact solution for creeping flow past a droplet under the assumption that the interfacial behavior could be described by the Newtonian surface fluid model and that surface tension and the two surface viscosities were independent of position and phase interface. The results of Boussinesq's analysis do not appear to be in any better agreement with available experimental data than those of Hadamard and Rybczynski. Neither the analysis of Boussinesq nor the theory of Hadamard and Rybczynski considers the effect of surfactant.

The significant effects of surface active material have been realized and been under extensive research only during the past 30 years. Savic (1953) first observed that when a bubble rises through a liquid containing surface active impurities, the fluid motion near its surface is slowed down or stopped. In some situations, a motionless film is adsorbed onto the rear part of the surface, while the remainder of the surface is practically free to move and has very little material adsorbed on it. Savic also began his theoretical study for the case of spherical drops moving at Reynolds numbers much smaller than unity, with negligible small interior viscosity and bearing rigid spherical caps. Savic's approximate numerical solution has been improved by Griffith (1962) and Davis and Acrivos (1966), who reported numerical difficulties for small caps under low Reynolds number flow. This cap model was further investigated by Harper (1973) through asymptotic solution for small Reynolds numbers. He obtained the drag coefficient from the value of a completely surfactant-free surface through a perturbation method, concluding that this model is often a good one if the surfactant is highly active and the Peclet number is high. Wasserman and Slattery (1969) also investigated the creeping flow past a fluid globule when a trace of surfactant is present; the result of a perturbation analysis show that the internal circulation and the free moving velocity are highly sensitive to small changes in surfactant concentration, although the bubble varies imperceptibly from a spherical shape. Recently, Sadal and Johnson (1983) obtained exact flow solutions for a fluid sphere with a surfactant cap in low Reynolds number flow. Lochiel (1965) presented empirical equations that predict the effect of small quantities of surfactants on mass transfer across a spherical interface for both small and large Reynolds numbers. The large Reynolds number solutions are valid only for bubbles. Levich (1962) presented an extensive analysis of the fall of a droplet under circumstances such that only the continuous phase contains surfactants in creeping flow.

Experimentally, Elzinga and Banchero (1961) observed that a tiny amount of fine solids of colloidal dimensions gradually collected at the interface and was swept around to the rear of the droplet. Kintner (1963), Harper (1972), and Clift et al. (1978) have reviewed the literature on the effects of surfactants on the motion and transport mechanism of bubbles and droplets. They have found that almost all the research has been done in the area of surfactant cap on a bubble in creeping flow condition. In the present study we are concerned with the droplets contaminated with monolayer insoluble surfactants. The contamination is slight and no surfactant cap is formed. A high Reynolds number flow is assumed. We have not found similar investigations in the literature.

ANALYSIS

We consider a droplet of density, ρ_l, dynamic viscosity, μ_l, and temperature, T_o, moving at a steady velocity, U_∞, in a quiescent pure vapor environment of temperature T_∞ ($T_\infty > T_o$) and atmospheric pressure. The condensing droplet is contaminated initially with surfactants that are relatively insoluble to both phases. Condensation is taking place on the surface of this droplet. Figure 1 shows the schematic of the system.

Basic assumptions in the analysis are as follows:

1. The fluid motion is steady. The vorticity diffusion time, R^2/ν_l, is typically at least one order of magnitude smaller than the droplet lifetime, τ_{life},

$$\tau_{\text{life}} = \rho_l c_p \Delta T (4/3)\pi R^3/(M/2\pi\bar{R}T)^{1/2}\Delta p(4\pi R^2)h_{fg}$$

where the driving force for pure steam condensation, Δp, is equal to $2\sigma\rho_g/\rho_l$, σ is the surface tension coefficient, and $\bar{R}$ is the universal gas constant. Since $(c_p\Delta T\rho_l)/(h_{fg}\rho_g) > 0(100)$ for this analysis, the vorticity diffusion time is at least one order of magnitude smaller than the droplet lifetime.

2. The droplet is initially contaminated with surfactant and the surfactant concentration distribution on the droplet surface is at steady state. The surfactant diffusion time, R^2/D_s, is also much smaller than τ_{life}.

3. The surfactant distributes as a monolayer on the droplet surface. This imposes a limitation on the maximum surfactant concentration or the total amount of surfactant. Beyond the limit, surfactant cap will be formed (Berg, 1972; Gaines, 1966).

4. The interface is smooth and is free of wavy motion due to surfactants.

5. The viscous dissipation, compressibility effects, and expansion work are neglected.

6. The droplet remains spherical.

7. The Reynolds number, $Re = U_\infty R/\nu_\infty$, is of the order of 100.

8. The effect of condensate on the droplet internal motion is negligible and the increase in droplet size is therefore also neglected due to the fact that the droplet radius will grow only around 1% (Chung and Chang, 1982).

9. The surfactant monlayer is always separating the liquid and vapor phases, i.e., the condensate penetrates the surfactant layer immediately after it reaches the surface. Swisher (1970) and Rosen (1978) discussed this phenomenon.

Since the vapor phase Reynolds number is assumed 0(100), the fluid motion inside the droplet will have a Reynolds number

$$Re_l = \frac{U_m R}{\nu_l}$$

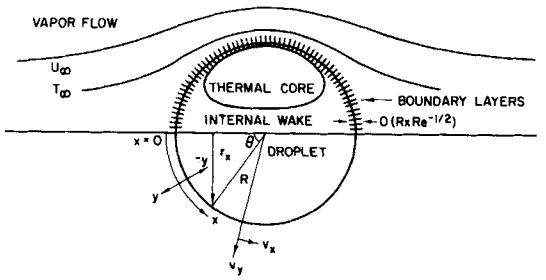

Figure 1. Schematic and coordinates system.

of the order of 100 even for $U_m/U_\infty = 0(10^{-2})$ because of the difference in kinematic viscosities. U_m is the liquid interface velocity at the equator ($\theta = 90°$) and it is the maximum velocity in the liquid phase. Therefore, the analysis of the liquid phase flow will also be based on the assumption of high Reynolds number. The validity of the assumption will be examined later. For high Re_l, three separate regions of flow can, in general, be discerned (Harper and Moore, 1968), i.e., a boundary-layer type flow near the surface of the droplet, an internal wake that follows the boundary layer, and an internal core that is surrounded by the boundary layer and the internal wake. The internal core is essentially inviscid and is represented by the Hill's vortex. See Figure 1 for schematics of the mathematical model.

Internal Core Region

Hill's vortex in the spherical coordinates with axisymmetric flow is given by the stream function (Milne-Thomson, 1968)

$$\psi_0 = -\tfrac{1}{2}Ar^2(R^2 - r^2)\sin^2\theta \tag{1}$$

where A is the strength of the vortex. In general, it is a function of the viscosity and density ratios between vapor and liquid phases. But it is also a function of the surfactant distribution at the interface for droplets contaminated with surfactants. The determination of this strength A is the main objective of this study.

The full strength, $A = (3/2)U_\infty/R^2$, was found to be the case of bubbles rising in a liquid environment (Clift et al., 1978). For oil droplets in gas surroundings, Prakash and Sirignano (1978) found that $(U_\infty)/(AR^2) = 0(10)$, i.e., the strength is one order of magnitude smaller than the full strength. But both analyses neglect the effects of surfactant. The current analysis is aimed at finding the strength for a contaminated condensing droplet moving in its own vapor. Due to the three-region structure of the liquid phase, the boundary-layer region has to be investigated first and then a matching of velocity at the common boundary between the boundary layer and the internal core is performed to determine the strength of the internal core.

Liquid Boundary Layer

The method similar to those used for the study of bubble motion (Harper and Moore, 1968) is also considered appropriate for the current problem. The boundary-layer flow is assumed basically a perturbed Hill's vortex motion, that is,

$$\bar{v} = \bar{v}_o + \bar{v}', \quad |v'| \ll |\bar{v}_o|$$
$$P = P_o + P', \quad P' \ll P_o \tag{2}$$

where the subscript o refers to Hill's vortex solution, and the prime refers to the perturbation. As indicated by Harper and Moore (1968), Hill's spherical vortex, $\bar{v}_o$, is an exact solution of the full Navier-Stokes equation, and at $r = R$, it is a streamline. But a discontinuity of shear stress will result at the interface if Hill's spherical vortex for the inside of the droplet and the potential flow for the outside are used. This explains the need for a perturbation solution.

Equation 2 should satisfy the following continuity and Navier-Stokes equations:

$$\nabla \cdot \bar{v} = 0 \tag{3}$$

$$\bar{v} \cdot \nabla\bar{v} = -(1/\rho_l)\nabla P + \nu_l \nabla^2 \bar{v} \tag{4}$$

As mentioned above, $\bar{v}_o$ and P_o also satisfy 3 and 4, therefore

$$\nabla \cdot \bar{v}' = 0 \tag{5}$$

$$\bar{v}' \cdot \nabla\bar{v}_o + \bar{v}_o \cdot \nabla\bar{v}' = -(1/\rho_l)\nabla P' + \nu_l \nabla^2 \bar{v}' \tag{6}$$

The Navier-Stokes equation is thus linearized.

Next, we rewrite Eqs. 5 and 6 in terms of curvilinear coordinates with x measuring along the droplet surface from the forward stagnation point and y normal to the droplet surface, outward as positive and inward as negative. We obtain

$$\frac{\partial}{\partial x}(v_x' R_x) + \frac{\partial}{\partial y}(v_y' R_x) = 0, \; R_x = R\sin\theta, \quad y = r - R \tag{7}$$

$$v_x' \frac{\partial v_{ox}}{\partial x} + v_y' \frac{\partial v_{ox}}{\partial y} + v_{ox}\frac{\partial v_x'}{\partial x} + v_{oy}\frac{\partial v_x'}{\partial y} = -\frac{1}{\rho_l}\frac{\partial P'}{\partial x} + \nu_l\left(\frac{\partial^2 v_x'}{\partial x^2} + \frac{\partial^2 v_x'}{\partial y^2}\right) \tag{8}$$

$$v_x' \frac{\partial v_{oy}}{\partial x} + v_y' \frac{\partial v_{oy}}{\partial y} + v_{ox}\frac{\partial v_y'}{\partial x} + v_{oy}\frac{\partial v_y'}{\partial y} = -\frac{1}{\rho_l}\frac{\partial P'}{\partial y} + \nu_l\left(\frac{\partial^2 v_y'}{\partial x^2} + \frac{\partial^2 v_y'}{\partial y^2}\right) \tag{9}$$

where $\bar{v}_o = (v_{ox}, v_{oy})$ and $\bar{v}' = (v_x', v_y')$. Under the assumption of high Reynolds number, the boundary-layer thickness, δ_l, is thin. Thus we can make the following simplification:

$$v_{ox} = -AR^2\left(1 - 2\frac{r^2}{R^2}\right)\sin\theta = AR^2\sin\theta \tag{10}$$

$$v_{oy} = AR^2\left(1 - \frac{r^2}{R^2}\right)\cos\theta = -2AR^2\left(\frac{y}{R}\right)\cos\theta, \quad y \le 0 \tag{11}$$

Before we substitute Eqs. 10 and 11 into Eqs. 8 and 9, Eqs. 8 and 9 have to be further simplified. Let us nondimensionalize Eqs. 7, 8, and 9 by using R for x and y, AR^2 for all velocity components, and $\rho_l U_\infty^2$ for pressure. The dimensionless Eqs. 7, 8, and 9 become

$$\frac{\partial}{\partial x}(v_x' \sin\theta) + \frac{\partial}{\partial y}(v_y' \sin\theta) = 0 \tag{12}$$

$$v_x' \frac{\partial v_{ox}}{\partial x} + v_y' \frac{\partial v_{ox}}{\partial y} + v_{ox}\frac{\partial v_x'}{\partial x} + v_{oy}\frac{\partial v_x'}{\partial y} = -\frac{\partial P'}{\partial x} + \frac{1}{Re_l}\left(\frac{\partial^2 v_x'}{\partial x^2} + \frac{\partial^2 v_x'}{\partial y^2}\right) \tag{13}$$

$$v_x' \frac{\partial v_{oy}}{\partial x} + v_y' \frac{\partial v_{oy}}{\partial y} + v_{ox}\frac{\partial v_y'}{\partial x} + v_{oy}\frac{\partial v_y'}{\partial y} = -\frac{\partial P'}{\partial y} + \frac{1}{Re_l}\left(\frac{\partial^2 v_y'}{\partial x^2} + \frac{\partial^2 v_y'}{\partial y^2}\right) \tag{14}$$

$$Re_l = (U_m R)/\nu_l, \quad U_m = AR^2$$

Next, let us assume that

$$v_x' = 0(\epsilon) \text{ and } \epsilon \ll 1 \tag{15}$$

Keeping only the terms of the order of ϵ, Eqs. 13 and 14 become

$$v_x' \frac{\partial v_{ox}}{\partial x} + v_{ox} \frac{\partial v_x'}{\partial x} + v_{oy} \frac{\partial v_x'}{\partial y} = -\frac{\partial P'}{\partial x} + \frac{1}{Re_l} \frac{\partial^2 v_x'}{\partial y^2} \tag{16}$$

$$\frac{\partial P'}{\partial y} = 0 \tag{17}$$

After substituting Eqs. 10 and 11, Eq. 16 becomes

$$v_x' \cos\theta + \sin\theta \frac{\partial v_x'}{\partial x} - 2y \cos\theta \frac{\partial v_x'}{\partial y} = -\frac{\partial P'}{\partial x} + \frac{1}{Re_l} \frac{\partial^2 v_x'}{\partial y^2} \tag{18}$$

In a curvilinear axisymmetric flow, the vorticity, ω', is defined as

$$\omega' = \frac{\partial v_y'}{\partial x} - \frac{\partial v_x'}{\partial y} \doteq -\frac{\partial v_x'}{\partial y} \tag{19}$$

Next, differentiate 17 with respect to x and 18 with respect to y and then take the difference between them. This results in the following vorticity equation:

$$-\omega' \cos\theta + \sin\theta \frac{\partial \omega'}{\partial x} - 2(\cos\theta) y \frac{\partial \omega'}{\partial y} = \frac{1}{Re_l} \frac{\partial^2 \omega'}{\partial y^2} \tag{20}$$

Introduce

$$W' = \frac{\omega'}{\sin\theta} \tag{21}$$

and

$$X = (2/3 - \cos\theta + (1/3)\cos^3\theta) \tag{22}$$

$$Y = (Re_l)^{1/2} y \sin^2\theta$$

Equation 20 becomes

$$\frac{\partial^2 W'}{\partial Y^2} = \frac{\partial W'}{\partial X} \tag{23}$$

It is noted that the boundary-layer vorticity Eq. 23 is not expected to be valid either close to the forward stagnation point ($X \sim 0$), where X is no longer of 0(1), or near the rear stagnation point ($X \sim 4/3$), where Y is not of $0(\delta)$. Some of the neglected terms may be of the same order as those retained.

The corresponding boundary conditions for Eq. 11 are discussed for Y = 0, droplet surface, $Y \to \infty$, inner boundary of the boundary layer, and the continuity equation between the forward and the rear stagnation points.

Y = 0, *droplet surface.* A shear stress balance equation at the interface is now developed for the liquid phase. Unlike most analyses, where surfactant-free systems were assumed, an additional force, $F_\sigma(\theta)$, due to the surfactant concentration variation, is added to the total force experienced by the liquid phase in addition to skin drag, $F_D(\theta)$, due to relative motion between liquid and vapor. It is noted F_σ and F_D are acting in opposite directions. Internal motion is induced by F_D, while F_σ slows it down.

$$\tau_{xy} = F_\sigma(\theta) + F_D(\theta) = \mu_l \left[\frac{\partial v_x}{\partial y} + \frac{\partial v_y}{\partial x}\right] \tag{24}$$

In terms of vorticity function, we obtain

$$W' = -3 + \frac{(F_\sigma(\theta) + F_D(\theta))/\sin\theta}{\mu_l AR} \tag{25}$$

$Y \to \infty$, *interface between core and boundary layer.* As required by a smooth match with the internal core flow, the perturbed vorticity, W', should be vanished at the interface of core and boundary layer:

$$W' \to 0 \text{ as } Y \to \infty \tag{26}$$

$X = X_o$, *starting point of boundary layer.* This boundary condition is specified at a small finite distance from the forward stagnation point, where Eq. 23 is approximately valid. Due to the looping motion of the flow field inside the droplet and the inviscid nature of the internal wake, a condition proposed by Harper and Moore (1968) is also appropriate here:

$$W'(X_o, Y) = W'(X_e, Y) = \gamma(Y) \tag{27}$$

Equation 27 indicates that the vorticity at the tail portion of the boundary layer ($X = X_e$, small finite distance before the rear stagnation point) is convected with no diffusion from near the rear stagnation point, through the internal wake, and back to the forward stagnation point region. This vorticity will reenter the front boundary layer at $X = X_o$.

The shear stress due to relative motion between liquid and vapor phases, $F_D(\theta)$, is generated from the boundary-layer analysis of the vapor phase; the details of the vapor phase calculation are given in Chung and Chang (1982).

The surfactant induced force, $F_\sigma(\theta)$, is evaluated based on a steady convection-diffusion balance model given by Levich (1962)

$$S = \nabla \cdot (\Gamma \bar{v}) - \nabla \cdot (D_s \nabla \Gamma) \tag{28}$$

where S is the source or sink for the case of soluble surfactants. Therefore, S is zero in this analysis of insoluble surfactants.

A fixed amount of surface active material initially adsorbed by the droplet will stay at the interface and will establish a steady state distribution according to Eq. 28. Γ is the surfactant surface concentration, and D_s is the coefficient of two-dimensional surface diffusion and is assumed a constant in this analysis. For a spherical droplet, Eq. 28 becomes

$$\frac{\partial}{\partial \theta}(\Gamma v_x \sin\theta) = \frac{D_s}{R} \frac{\partial}{\partial \theta} \sin\theta \frac{\partial \Gamma}{\partial \theta} \tag{29}$$

Integrating Eq. 29 from $\theta = 0$ to $\theta = \theta$, it becomes

$$\frac{\partial \Gamma}{\partial \theta} = \frac{R\Gamma}{D_s} v_x \tag{30}$$

It has been well accepted that, for a dilute monolayer surfactant (Berg, 1972)

$$-\frac{\partial \sigma}{\partial \Gamma} = \bar{R}T \tag{31}$$

where σ is the surface tension, $\bar{R}$ is universal gas constant, and T is absolute temperature.

Using Eq. 31, we rearrange Eq. 30 as follows:

$$-\frac{\partial \sigma}{\partial \theta} = \frac{\bar{R}T}{D_s} R\Gamma v_x \tag{32}$$

Solving Γ from Eq. 30, Eq. 32 becomes

$$F_\sigma(\theta) = \frac{-1}{R} \frac{\partial \sigma}{\partial \theta} = \frac{\bar{R}T}{D_s} \Gamma_o AR^2 \sin\theta [\exp(Pe_s(1 - \cos\theta))] \tag{33}$$

where Γ_o is the surfactant concentration at $X = X_o$, and Pe_s is the interface mass transfer Peclet number, which is defined as $R \cdot AR^2/D_s$.

SOLUTION PROCEDURE

The solution of Eq. 23 was obtained from Carslaw and Jaeger (1973) and is as follows:

$$W' = \frac{1}{2(\pi X)^{1/2}} \int_0^\infty \gamma(Y')[\exp(-(Y - Y')^2/4X) - \exp(-(Y + Y')^2/4X]dY' - 3\text{erfc}(Y/2X^{1/2}) + \phi(X,Y) \quad (34)$$

where $\phi(X,Y)$ is the particular solution corresponding to the second term on the right-hand side of Eq. 25. It is noted that $\phi(X,Y)$ is also a function of AR^2 implicitly. Due to the analytical nature of Eq. 34, the second term of Eq. 25 was numerically fitted with third-order polynomial of X. The fitting was done sectionally because the reverse in sign for the total drag force after the separation point where the drag from vapor phase is negligibly small and the surface tension drag is dominant.

The iteration cycle for evaluating AR^2 is now explained as follows:

1. First, an initial guess was made for the Hill vortex strength, AR^2.
2. Evaluate the shear stress due to the vapor phase. This requires another interaction cycle in the vapor boundary analysis; it is discussed in more detail in Chung and Chang (1982).
3. Obtain $F_\sigma(\theta)$ from Eq. 33.
4. Solve for a new AR^2 from Eq. 34. The procedure is outline below.

Based on Eq. 27, we write Eq. 34 in the following form:

$$\frac{1}{2(\pi X_e)^{1/2}} \int_0^\infty \gamma(Y')[\exp(-Y - Y')^2/4X_e) - \exp(-(Y + Y')^2/4X_e)]dY' - 3\,\text{erfc}(Y/2X_e^{1/2}) + \phi(X_e,Y) = \gamma(Y) \quad (35)$$

Following the procedure from Harper and Moore (1968), Eq. 35 is further rearranged into g_1 and g_2, such that

$$\gamma(Y) = 3g_1(Y) + \frac{AR^2}{U_\infty} g_2(Y) \quad (36)$$

and

$$g_1(Y) = \frac{1}{2(\pi X_e)^{1/2}} \int_0^\infty g_1(Y')[\exp(-(Y - Y')^2/4X_e) - \exp(-(Y + Y')^2/4X_e)]dY' - \text{erfc}(Y/2X_e^{1/2}) \quad (37)$$

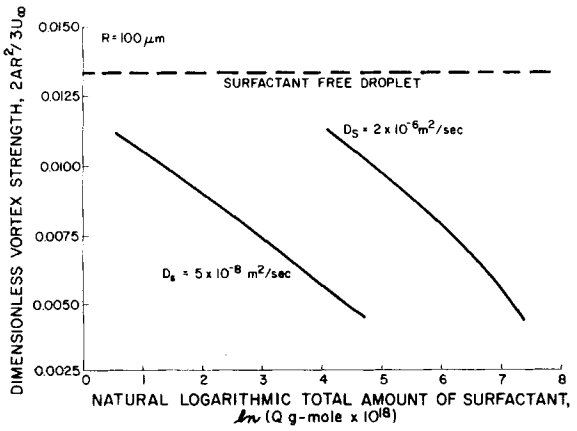

Figure 2. Vortex strength of internal motion vs. total amount of surfactant for 100 μm droplets.

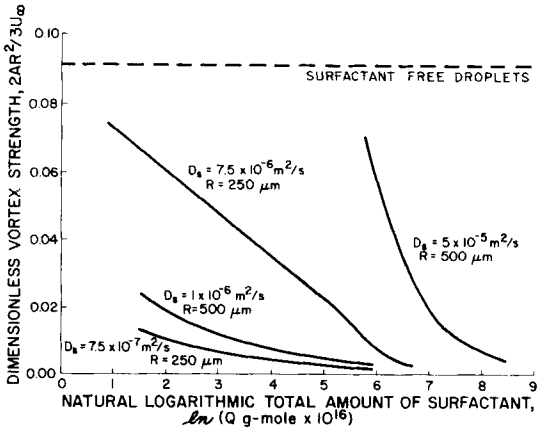

Figure 3. Vortex strength of internal motion vs. total amount of surfactant for 250 and 500 μ droplets.

$$g_2(Y) = \frac{1}{2(\pi X_e)^{1/2}} \int_0^\infty g_2(Y')[\exp(-(Y - Y')^2/4X_e) - \exp(-(Y + Y')^2/4X_e)]dY' + \frac{U_\infty}{AR^2}\phi(X_e,Y) \quad (38)$$

Equations 37 and 38 were solved iteratively. The updated Hill vortex strength was then obtained according to Eq. 26:

$$AR^2 = -U_\infty \frac{3g_1(Y \to \infty)}{g_2(Y \to \infty)} \quad (39)$$

5. Check whether the two successive iterates of AR^2 satisfy the convergence criterion.

RESULTS AND DISCUSSION

Parametric calculations were performed for condensing water droplets moving in their own vapor with different amounts of surfactant contamination. The ambient vapor temperature is 150°C; the droplet initial temperature, 75°C. Detailed information on condensation heat and mass transfer is given in Chung and Chang (1982). Droplet radius investigated ranges from 100 to 1000 μm, which result in flows in the high Reynolds number regime. The information on diffusion coefficients of a surfactant monolayer is very limited in the literature. The only useful data found were

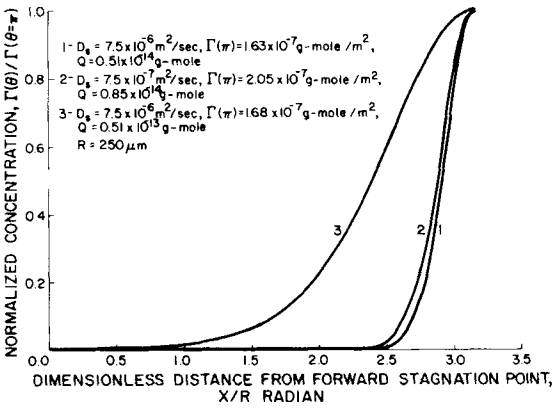

Figure 4. Surfactant concentration along the droplet surface.

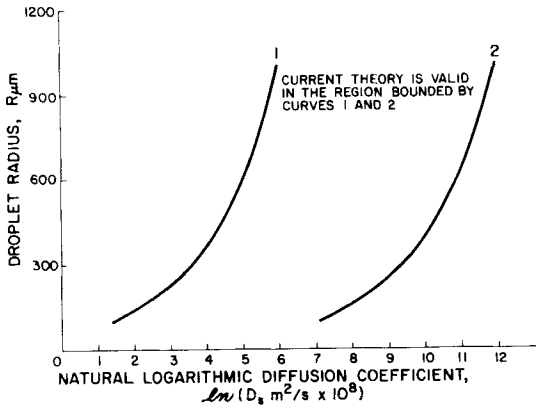

Figure 5. Region of validity for current theory.

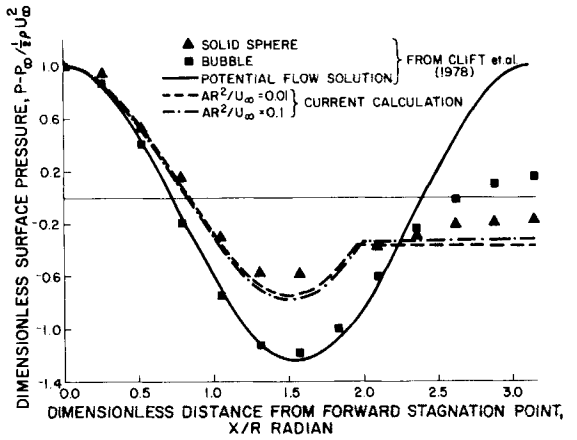

Figure 6. Comparison of drag coefficients among contaminated droplets, solid spheres, and air bubbles.

the experimental measurements of Sakata and Berg (1969). They reported diffusion coefficients ranging from 10^{-9} to 10^{-8} m^2/s for myristic acid monolayer film in liquid phase on a water substrate. They also concluded that the diffusion coefficient strongly depends on the phase of the monolayer. They did not report any diffusion coefficient for gaseous phase surfactant film. It was estimated that the diffusion coefficients for gaseous type monolayer would be as high as 10^{-3} m^2/s based on two-dimensional Stokes-Einstein relation. Therefore, the diffusion coefficients vary from 10^{-9} to 10^{-3} m^2/s in present parametric calculations.

Figures 2 and 3 show the variations of the normalized vortex strength as a function of the total amount of surfactant, Q in gmol, at the interface. The vortex strength is normalized by the full strength of Hill's vortex, i.e., $3/2U_\infty$. The horizontal dashed lines in the upper portion of these figures represent the normalized vortex strength for identical system conditions except the droplet is surfactant free. These dashed lines provide a direct comparison of the effects of surfactant on the strength of vortex. It is apparent that surfactants with lower surface diffusion coefficients are more effective in weakening the strength of internal circulation. This may be explained by the surfactant transport mechanism on the droplet surface. Surfactants are generally brought toward the rear stagnation point by the surface convective motion, while an equal amount of the surfactant has to be transported toward the forward stagnation point by diffusion process to maintain a balance at steady state. Therefore, a very steep concentration gradient is required for the diffusive back flow to balance the more efficient convective flow. Therefore, the smaller the surface diffusive coefficient, the steeper the surfactant concentration gradient and, in turn, a higher surface tension gradient to slow down the internal motion. An expected general trend is that more surfactant on the droplet surface always results in slower internal motion because the concentration gradient covers more surface area, as shown in Figure 4.

Figure 4 plots the normalized surfactant concentration along the droplet surface. Surfactant concentration is normalized, based on its value at the near stagnation point. Curves 1 and 2 examine the effects of different surface diffusion coefficients for 250 μm droplets where curve 1 with D_s equal to 7.5×10^{-6} m^2/s and curve 2 with D_s equal to 7.5×10^{-7} m^2/s. It is interesting to note that curve 1 and curve 2 are very similar to each other, which may be explained as follows: D_s for curve 1 is ten times larger than that of curve 2 and vortex strength for curve 1 is about ten times larger than that of curve 2, as shown in Figure 3. Therefore, faster convection with larger D_s will result in similar surfactant concentration distribution to that of slower convection with smaller D_s for droplets of the same radius. This may also be seen from Eq. 33

$$\Gamma = \Gamma_o \exp[Pe_s(1 - \cos\theta)], \quad Pe_s = R \cdot AR^2/D_s \qquad (40)$$

where AR^2/D_s is the unique parameter for a given R.

Curve 3 was plotted to compare with curve 1 for a different total amount of surfactant. For the same D_s, more total amount of surfactant on the droplet corresponds to much more surface area with concentration gradient and less steep surfactant concentration variations along the droplet surface. In general, the surfactant concentration exhibits a sharp rise after the equator ($\theta = 90°$) and the surfactant concentration is negligibly small before the sharp rise. This is typical of the convection-diffusion balance system as explained above.

Attention should also be given to the limits of current analysis. First, the surfactant concentration should not be lower than those that would invalidate the continuum assumption adopted for the surfactant transport mechanism. This lower limit was established based on the microscopic theory that the two-dimensional mean free path of surfactant molecules is small compared with the droplet radius. The above theory requires that the surfactant concentration be larger than 10^{-12} mol/m^2. The upper limit of surfactant concentration was based on the theory that if the surfactant molecules are too dense to maintain a monolayer film, then they will collapse into a thick immobile layer, and the current model also becomes invalid.

Many researchers have addressed the problem of an immobile cap on a bubble or a drop in low Reynolds number flow. Berg (1972) provided a criterion for the collapse of monolayer on water. The upper limit was found to be around 10^{-5} mol/m^2 for this investigation. All the cases reported here are within the limits given above. Since the surface concentration depends strongly on the

TABLE 1

	C_p	C_F	C_D
Rigid Sphere[1]	0.5100	0.5900	1.0960
Water Drop in Air[1]	0.4900	0.5900	1.0800
$\frac{AR^2}{U_\infty} = 0.01^2$	0.4899	0.6671	1.1617
0.02^2	0.4913	0.6634	1.1609
0.066^2	0.4698	0.6438	1.1268
0.111^2	0.4450	0.6235	1.0885
Bubble[1]	0.1810	0.2240	0.4050

[1] Data from Clift et al. (1978).
[2] Current calculations.

diffusion coefficient, the range where the current theory is valid as a function of the diffusion coefficient was plotted in Figure 5. The area bounded by the two solid lines is the region of validity. This plot was obtained by requiring the concentration at the front stagnation point by 10^{-12} mol/m^2 and the concentration at the rear stagnation point does not exceed 10^{-5} mol/m^2.

It is also interesting to examine the drag coefficient and the surface pressure distribution of a contaminated condensing droplet. The form drag coefficient, C_p, the friction drag coefficient, C_F, and the total drag coefficient, C_D, defined as the total drag force divided by $\frac{1}{2}\rho U_\infty^2$, are given in Table 1 for a contaminated condensing droplet with vortex strength (AR^2/U_∞) of 0.01, 0.02, 0.066, and 0.111. Also given in Table 1 is the corresponding drag coefficients for noncondensing and surfactant free rigid sphere, water drop in air, and gas bubble (Clift et al., 1978). The formulas for calculating these coefficients of a condensing droplet are given by Sadal and Ayyaswamy (1983). The drag coefficient, due to momentum flux, which is nonzero for condensing droplets because of its nonzero interfacial normal velocity, is not given in the table. It is two orders of magnitude smaller than C_p and C_F. It is seen from Table 1 that C_P is smaller and C_F is larger compared to water drop in air without condensation, which is mainly due to the condensation-induced normal interfacial velocity, and the total drag coefficient is also larger. But, for condensing droplets, C_p, C_F, and C_D, all decrease with increasing AR^2/U_∞. Figure 6 shows the dimensionless surface pressure distributions for condensing droplets with different vortex strengths up to the point of flow separation because the current model is not valid after the separation point. Pressure distributions for bubble and solid sphere and that calculated from potential flow are also included for comparison. As expected, the surface pressure distributions of condensing droplets fall between those of a solid sphere and a gas bubble. Also noted is that these calculated pressure distributions are closer to that of a solid sphere as the droplet is more like a solid sphere than a gas bubble. This is explained further because the pressure distribution of the droplet with weaker internal motion, $AR^2/U_\infty = 0.01$, is closer to that of a solid sphere than that of the droplet with $AR^2/U_\infty = 0.1$.

ACKNOWLEDGMENT

This research work was supported through a National Science Foundation Grant CME-8006762. We appreciate many meaningful discussions and suggestions from T. E. Carleson of the University of Idaho.

NOTATION

A = strength of Hill's vortex
C_D = drag coefficient
C_F = friction drag coefficient
C_p = pressure drag coefficient
c_p = specific heat at constant pressure
D_{12} = binary diffusion coefficient
D_s = surface diffusion coefficient of the surfactants
$F_D(\theta)$ = skin drag force
$F_\sigma(\theta)$ = surface tension gradient force
$g_1(Y)$ = unknown function of (Y) used in Eq. 36
$g_2(Y)$ = unknown function of (Y) used in Eq. 36
h_{fg} = latent heat of vaporization
P = pressure
Pe_s = surface Peclet number ($=R\,AR^2/D_s$)
Pr = Prandtl number ($= C_p/K$)
Q = total amount of surfactant on the droplet surface
R = droplet radius
$\bar{R}$ = universal gas constant
r = radial distance from the droplet center
Re_l = Reynolds number ($= U_\infty R/\nu$)
Re = liquid phase Reynolds number ($= U_m R/\nu_l$)
r_x = normal distance fom the axis of symmetry
S = sink or source in Eq. 28
T = absolute temperature at the interface
T_o = droplet initial temperature
T_∞ = ambient temperature
U_m = maximum interfacial velocity
U_∞ = free stream velocity
$\bar{v}$ = velocity vector in the liquid boundary layer
v_x = tangential velocity component in the liquid boundary layer
v_y = normal velocity component in the liquid boundary layer
W' = transformed nondimensional perturbation vorticity defined in Eq. 21
X = transformed coordinate of θ defined by Eq. 22
x = curvilinear coordinate along the drop surface
Y = transformed coordinate defined in Eq. 22
y = normal coordinate from the droplet surface

Greek Letters

Γ = surfactant surface concentration
Γ_0 = surfactant surface concentration at $X = X_0$
$\gamma(Y)$ = unknown function of Y used in Eq. 35
δ_l = dimensionless liquid boundary-layer thickness
ϵ = small parameter representing the order of magnitude of the perturbed quantities
θ = tangential coordinate in spherical coordinates
μ = dynamic viscosity
ν = kinematic viscosity
ρ = density
τ = time
$\phi(X,Y)$ = particular solution of Eq. 23 corresponding to the second term of the right-hand side of Eq. 25
σ = surface tension coefficient
ψ_o = Hill's vortex stream function
ω' = nondimensional perturbation vorticity

Subscripts and Superscript

l = liquid phase
o = Hill's vortex solution
x = tangential component
y = normal component
∞ = ambient, far away from the droplet
$'$ = perturbation component

LITERATURE CITED

Berg, J. C., "Interfacial Phenomenon in Fluid Phase Separation Process, *Recent Development in Separation Science*, CRC Press, 1 (1972).

Boussinesq, J., "Vitesse de la chute lente, devenue uniforme, d'une goutte liquide spherique, dans un fluide visqueux de poids specifique moindre" (The Uniform Velocity of a Slow Falling Spherical Liquid Droplet in a Viscous Fluid of Lesser Specific Weight), *Ann. Chim. Phys.*, **29**, 364 (1912).

Carslaw, H. S., and J. C. Jaeger, *Conduction of Heat in Solids*, Oxford University Press, Oxford, 59 (1973).

Chung, J. N., and Tae-Ho Chang, A Mathematical Model of Condensation Heat and Mass Transfer to a Moving Droplet in Its Own Vapor," *ASME J. Heat Transfer*, *106*, 417 (1984).

Clift, R., J. R. Grace, and M. E. Weber, *Bubbles, Drops, and Particles*, Academic Press, New York, 35 (1978).

Davis, R. E., and A. Acrivos, "The Influence of Surfactant on the Creeping Motion of Bubbles," *Chem. Eng. Sci.*, **21**, 681 (1966).
Elzinga, E. R., and J. T. Banchero, "Some Observations on the Mechanics of Drops in Liquid-Liquid Systems," *AIChE J.*, **7**, 394 (1961).
Gaines, G. L., Jr., *Insoluble Monolayers at Gas Liquid Interface*, Interscience, New York, 144 (1966).
Griffith, R. M., "The Effect of Surfactants on the Terminal Velocity of Drops and Bubbles," *Chem. Eng. Sci.*, **17**, 1057 (1962).
Hadamard, J., "Mouvement permanent lent d'une sphere liquide et visqueuse daus un liquide visqueux" (The Slow Steady Movement of Viscous Liquid Sphere in a Viscous Liquid), *Compt. Rend. Acad. Sci.*, **152**, 1735 (1911).
Harper, J. F., "The Motion of Bubbles and Drops Through Liquids," *Advances in Applied Mechanics*, **12**, Academic Press, New York, 59 (1972).
——, "On Bubbles with Small Immobile Adsorbed Films Rising in Liquids at Low Reynolds Number," *J. Fluid Mech.*, **58**, 539 (1973).
——, "Surface Activity and Bubble Motion," *Appl. Sci. Res.*, **38**, 143 (1982).
Harper, J. F. and D. W. Moore, "The Motion of a Spherical Liquid Drop at High Reynolds Number," *J. Fluid Mech.*, **32**, 367 (1968).
Kintner, R. C., "Drop Phenomena Affecting Liquid Extraction," *Advances in Chemical Engineering*, **4**, Academic Press, New York and London (1963).
Levich, V. G., *Physicochemical Hydrodynamics*, Prentice-Hall, Englewood Cliffs, NJ, 409 (1962).
Lochiel, A. C., "The Influence of Surfactants on Mass Transfer Around Spheres," *Can. J. Chem. Eng.*, **43**, 140 (1965).
Milne-Thomson, L. M., *Theoretical Hydrodynamics*, Macmillan, New York, 578 (1968).
Prakash, S., and W. A. Sirignano, "Liquid Fuel Droplet Heating with Internal Circulation, *Intern. J. Heat Mass Transfer*, **21**, 880 (1978).
Rybczynski, W., "On the Translatory Motion of a Fluid Sphere in Viscous Medium," *Bull. Intern. Acad. Pol. Sci. Lett. Cl. Sc. Math. Natur. Ser. A*, 40 (1911).
Rosen, M. J., *Surfactants and Interfacial Phenomena*, Wiley, New York (1978).
Sadal, S. S., and P. S. Ayyaswamy, "Flow Past a Liquid Drop with a Large Non-Uniform Radial Velocity," *J. Fluid Mech.*, **133**, 65 (1983).
Sadal, S. S., and R. E. Johnson, "Stokes Flow Past Bubbles and Drops Partially Coated with Thin Films. I. Stagnant Cap of Surfactant Film-Exact Solution," *J. Fluid Mech.*, **126**, 237 (1983).
Sakata, E. K., and J. C. Berg, "Surface Diffusion in Monolayers," *Ind. Eng. Chem. Fund.*, **8**, 570 (1969).
Savic, P., "Circulation and Distortion of Liquid Drops Falling Through a Viscous Medium," *Natl. Res. Council, Canadian Div., Mech. Eng., Rept. MT-22* (1953).
Swisher, R. D., *Surfactant Biodegradation*, Dekker, New York, 32 (1970).
Wasserman, M. L., and J. C. Slattery, "Creeping Flow Past a Fluid Globule When a Trace of Surfactant Is Present," *AIChE J.*, **15**, 533 (1969).

Manuscript received Nov. 18, 1983; revision received Sept. 10, 1984 and accepted Sept. 11.